Continuous-time co-operation of integrated electricity and natural gas systems with responsive demands under wind power generation uncertainty

Author(s): Nikoobakht, Ahmad; Aghaei, Jamshid; Shafie-khah, Miadreza; Catalão, J. P. S.

Title: Continuous-time co-operation of integrated electricity and natural gas systems with responsive demands under wind power generation uncertainty

Year: 2020

Version: Accepted manuscript

Please cite the original version:

Nikoobakht, A., Aghaei, J., Shafie-khah, M., & Catalão, J.P.S., (2020). Continuous-time co-operation of integrated electricity and natural gas systems with responsive demands under wind power generation uncertainty. *IEEE transactions on smart grids*. https://doi.org/10.1109/TSG.2020.2968152

Continuous-Time Co-Operation of Integrated Electricity and Natural Gas Systems with Responsive Demands Under Wind Power Generation Uncertainty

Ahmad Nikoobakht, *Member, IEEE,* Jamshid Aghaei, *Senior Member, IEEE,* Miadreza Shafie-khah, *Senior Member, IEEE,* and J.P.S. Catalão, *Senior Member, IEEE*

***Abstract*—This paper studies the role of electricity demand response program (EDRP) in the co-operation of the electric power systems and the natural gas transmission system to facilitate integration of wind power generation. It is known that time-based uncertainty modeling has a critical role in co-operation of electricity and gas systems. Also, the major limitation of the hourly discrete time model (HDTM) is its inability to handle the fast sub-hourly variations of generation sources. Accordingly, in this paper, this limitation has been solved by the operation of both energy systems with a continuous time model (CTM). Also, a new fuzzy information gap decision theory (IGDT) approach has been proposed to model the uncertainties of the wind energy. Numerical results on the IEEE Reliability Test System (RTS) demonstrate the benefits of applying the continuous-time EDRP to improve the co-scheduling of both natural gas and electricity systems under wind power generation uncertainty.**

***Index Terms*—Demand response program, continuous-time model, natural gas system, IGDT method, wind energy.**

NOTATION

A. Indices

q	Index of Bernstein basis function.
w, g, s	Index for wind farms, generation units, and natural gas storage, respectively.
i, j	Index of nodes in natural gas system.
p	Index of natural gas pipeline.
t	Index of continuous-time.
t'	Index of discrete-time.
ℓ	Index of linear blocks.
$(\bullet)_{(\cdot),t}$	Related to element $(\cdot)$ at time period t.
Ω_c	Sets of natural gas pipelines with compressor.

B. Parameters

c_g	Cost of the generating unit.
c_n	Cost of the demand response at bus n.
c_g^{su}	Startup cost of the generating unit .
$\overline{\dot{G}}_g/\underline{\dot{G}}_g$	Max/min output of the generating unit.
$\underline{\dot{D}}_n/\overline{\dot{D}}_n$	Min/max ramp rate for the flexible demand.
$\overline{W}_{wt}/\overline{D}_{nt}$	Forecasted wind power/load.
b_{nm}	Susceptance of transmission line $k(n,m)$.
$\overline{f}_k$	Maximum power flow on a transmission line.
ΔE_n	Maximum energy change of a flexible demand in the daily scheduling.
$\Delta\Phi^{\pm}$	Permissible power adjustment of flexible demand.
L_{it}	Natural gas demand.
L_{it}^n	Residential natural gas demand.
L_{it}^e	Natural gas demand for natural gas-fired generation.
$\underline{\rho}_i/\overline{\rho}_i$	Min/max square of node pressures.
$\underline{\pi}_i/\overline{\pi}_i$	Min/max node pressures.
$\varphi_{\ell,p}, \gamma_{\ell,p}$	Constants in the ℓth linear block.
$\underline{f}_{\ell,p}/\overline{f}_{\ell,p}$	Min/max natural gas flow for the ℓth linear block.
$\underline{g}_i/\overline{g}_i$	Min/max limit on natural gas supply.
Θ_p	Pipeline constant.
λ_p	Compressor factor for a pipeline with compressor.
$\underline{E}_s/\overline{E}_s$	Min/max storage volume.
$\underline{S}_s^{in}/\overline{S}_s^{in}$	Min/max storage input.
$\underline{S}_s^{out}/\overline{S}_s^{out}$	Min/max storage output.
$\underline{\dot{S}}_s^{out}/\overline{\dot{S}}_s^{out}$	Min/max ramp rate for storage outflow.
$\underline{\dot{S}}_s^{in}/\overline{\dot{S}}_s^{in}$	Min/max ramp rate for storage inflow.
α, β, γ	Coefficients of natural gas function of gas-fired generation.
$B_{q,Q}^t$	Bernstein basis function of order Q.
$\Phi_{Q_m}^{x_t}$	Bernstein polynomial operator takes a function x_t .

The work of M. Shafie-khah was supported by FLEXIMAR-project (Novel marketplace for energy flexibility), which has received funding from Business Finland Smart Energy Program, 2017-2021. J.P.S. Catalão acknowledges the support by FEDER funds through COMPETE 2020 and by Portuguese funds through FCT, under POCI-010145-FEDER-029803 (02/SAICT/2017).

A. Nikoobakht is with the Higher Education Center of Eghlid, Eghlid, Iran- (email: a.nikoobakht@eghlid.ac.ir).

J. Aghaei is with the Department of Electrical and Electronics Engineering, Shiraz University of Technology, Shiraz, Iran (e-mail: aghaei@sutech.ac.ir).

M. Shafie-khah is with School of Technology and Innovations, University of Vaasa, 65200 Vaasa, Finland (*first corresponding author*, e-mail: mshafiek@univaasa.fi).

J.P.S. Catalão is with the Faculty of Engineering of the University of Porto and INESC TEC, Porto 4200-465, Portugal (*second corresponding author*, e-mail: catalao@fe.up.pt).

$C_{Q_m}^{(\bullet)}$	Bernstein coefficient of $(\bullet)$.
Q	Order of Bernstein polynomial.
M	Large enough constant.
Λ_Ω	Cost threshold.
σ_Ω	Percent of cost threshold.

$C.Variables$

G_{gt}	Output power of a generating unit.
D_{nt}	Scheduled load for flexible demand.
ΔD_{nt}^{+}/ ΔD_{nt}^{-}	Increase /decrease flexible demand.
ρ_{it}	Pressure.
$z_{g,t}/y_{gt}$	Shutdown/startup binary variables for generating unit.
S_{st}^{in}/S_{st}^{out}	Storage inflow/outflow.
$\dot{S}_{st}^{in}/\dot{S}_{st}^{out}$	Inflow/outflow ramping routes.
I_{gt}	Binary variable for generating unit state.
$\nu_{\ell pt}$	Binary indicator for the ℓth linear block.
Θ	Total operation cost [$].
$\dot{G}_{gt}$	Ramp up rate for generating unit.
$f_{\ell pt}$	Natural gas flow at pipeline p for the ℓth linear block.
f_{pt}	Natural gas flow at a pipeline.
g_{it}	Natural gas supply.
f_{kt}	Power flow on a transmission line.
θ_{nt}	Voltage angle at a bus.
E_{st}	Storage volume for natural gas storage.
λ	Radius of wind power uncertainty.
$\mu_{(\cdot)}(\cdot)$	Fuzzy membership function.
$\beta_{r/o}$	Overall satisfaction for membership function of risk averse and opportunity seeker strategies.
$\vec{C}_{Q_m}^{(\bullet)}$	Vector containing Bernstein coefficients of $(\bullet)$.
W_{wt}	Actual available wind power generation.

$D.Acronyms$

WEG	Wind energy generation.
SO	System operator.
NGFG	Natural gas-fired generation.
NGS	Natural gas system.
EDRP	Electricity demand response programs.
UC	unit commitment.
SCUC	Security constrained unit commitment
HDTM	Hourly discrete-time model.
CTM	Continuous-time model.
SM	Stochastic model.
RM	Robust model.
IGDT	Information-gap decision theory.
F-IGDT	Fuzzy IGDT
BP	Bernstein polynomial.
NGSU	Natural gas storage units.
RA	Risk-averse.
TC	Total cost.
SOC	State of charge.
OS	Opportunity seeker.
DM	Decision maker.
GU	Generator unit.
DT-EDRP	Discrete-time EDRP.
CT-EDRP	Continuous-time EDRP.
NGC	Natural gas consumptions .

I. Introduction

A. Aim and motivation

TODAY , wind energy generations (WEGs) are an important resource in the power systems operation, and plays a key role in the power generation. But, the main challenge faced by many system operators (SOs) is the operation of power systems under fast sub-hourly variations and uncertainty of WEGs [1].

The first option that the SO could choose to decrease uncertainty and fast sub-hourly variations of WEG in power systems is wind energy spillage, however, this option is unattractive. Alternative solution is to use a generating unit that it has fast startup and ramping capabilities to cover the fast variations and uncertainty of WEGs. For this purpose, the natural gas-fired generations (NGFGs) can contribute as a fast start and ramp unit.

However, there is a challenge whether the NGFGs can be supplied by the natural gas transmission system in the case it is committed to have power generation. For the reason that the operation of NGFG highly relies on the interruptible natural gas systems (NGSs).

Indeed, the supply interruption of NGSs occurs during peak load periods in cold seasons once they are scheduled to supply residential and commercial customers for heating purposes [2]. Besides, the fuel curtailment could lead to NGFGs shutdown, higher power system operation costs, and even jeopardize power system security [3].

This is expected, because the NGFG is an important component in the providing flexible ramp capacity in power systems, and plays a key role to mitigate fast variations and uncertainty of WEGs. Accordingly, the availability of the natural gas supply would directly affect the power system operation in terms of cost, scheduling, and integrating WEGs [4].

It seems the main strategy to reduce the impacts of interruptible natural gas transmission constraints on the electricity system could be reduced the contribution of NGFGs in the generation scheduling. However, if the contribution of NGFGs in generation is reduced, the SO could not mitigate the sub-hourly variations and uncertainty of WEGs.

In this condition, electricity demand response programs

(EDRPs) can contribute to follow the sub-hourly variability and uncertainty of WEGs by increase fast ramping up and down capacities in power system.

However, two main questions in co-operation of electricity and natural gas transmission systems must be addressed in this study:

(i) How to manage fast sub-hourly variations of WEGs and fast ramping capability of the NGFGs and EDRPs in electrical power system.

(ii) How to model uncertainty of WEGs in electrical power system operation.

The co-operation of electricity and natural gas transmission systems is handled by solving the unit commitment (UC) problem which schedules the set of the NGFGs on an hourly basis, to meet the hourly forecasted load and cover hourly variations of forecasted load.

The current UC model has worked well for compensating the variability and uncertainty of load in the past, but it is starting to fall short, as increasing WEGs add sub-hourly variability to the power system and large sub-hourly ramping events happen much more commonly. Also, it is impossible to instantaneously ramp up/down at the hourly intervals, thus, with the UC model cannot manage sub-hourly variations of WEGs and ramping capability of NGFGs in electrical power system.

In this condition, the scarcity of ramping resources is occurred. The scarcity of ramping resources is a phenomenon that occurs once the electrical power system has enough ramping capacity but it is unable to acquire ramping requirements to respond to sub-hourly WEG variations.

In recent years, there has been an increasing interest in co-operation of electricity and natural gas transmission systems [5]-[11].

A cooperative model has been proposed in [5] to assess the impacts of interruptible natural gas transmission systems on electricity system security. The cooperated scheduling of interdependent natural gas transmission system and hydrothermal power system has been investigated by [6].

The short-term integrated operation of interdependent electric and natural gas systems has been considered in [7]. A combined nonlinear model for security constrained unit commitment (SCUC) problem including the constraints of natural gas transmission has been developed in [8].

Similarly, a coordinated day-ahead scheduling of water and natural gas systems has been proposed in [9] while characterizing the uncertainties of units/transmission lines outage, water inflow and electricity load be means of a two-stage stochastic optimization framework.

Besides, in [10], a coordinated stochastic model has been suggested to consider interdependencies of electricity and natural gas transmission systems taking hourly electricity load forecast errors and random outages of generating units/transmission lines into account.

A security-constrained bi-level economic dispatch model has been proposed in [3] for co-operation of electricity and natural gas systems including wind energy and power-to-gas procedure.

In [11], the impacts of natural gas constraints on the stochastic day-ahead electricity markets of energy and reserve have been assessed. Also, it investigates the effect of WEG uncertainty on the co-operation of electricity and gas systems.

Above mentioned research studies, i.e., [5]-[11], in the field of co-operation of electricity and natural gas systems with (without) fast variations of WEG, have only focused on the hourly discrete-time model (HDTM).

The HDTM is suitable for only hourly commitment decision points and capturing hourly ramping flexibility of NGFGs and EDRPs, but, sub-hourly generation schedules and the sub-hourly ramping flexibility of the NGFGs and EDRPs cannot be captured by current HDTM.

In order to address first question, in this study, a continuous-time model (CTM) based on Bernstein polynomial functions is adopted which allows to better capture the ramping capability of the NGFGs and EDRPs because it provides a more accurate representation of the sub-hourly ramping needs to follow sudden sub-hourly variations of WEGs. Also, the application of the CTM in the proposed problem can modify the co-operation of electricity and gas systems, and coordinate the NGFGs and EDRPs to have a better response to the real-time sudden changes of the WEGs and load.

Recently, researchers have shown an increased interest in continuous-time model [12] and [13].Compared to papers [12] and [13]on the continuous-time model, here we extend that work in three important directions, (a) by modeling a multi-bus system with continuous-time flows across transmission lines (b) by modeling fast-ramping resources, i.e., the NGFGs and EDRPs, in continuous-time framework, (c) with a more generic formulation not only limited to electricity transmission system but also for natural gas systems can be utilized.

The CTM is appropriate for manage the sub-hourly variations of WEGs, but the WEG uncertainty cannot be captured by this model. In this context, the problem of uncertainty modelling of WEG is still an important issue. Therefore, another objective of this study is to propose a new method to address WEG uncertainty in electricity power systems.

The available uncertainty models for WEG are categorized into three classifications:

Stochastic model (SM): Most studies in the field of uncertainty modelling of WEG have only focused on the SM, it defines the uncertain parameters by means of scenarios [10], [13]. Hence, the optimal solution of an operation problem with SM is only guaranteed to be feasible for the scenarios considered in the problem. Furthermore, the complex optimization problem depends on the number of scenarios. Consequently, the operation problem with the SM faces two key challenges:

(i) The SM needs a large number of scenarios to model the wind uncertainty which results in increase size of problem and high execution time [13].

(ii) The optimal solution of proposed co-operation problem with SM is dependent on the accuracy of statistical data. Noted that, the statistical data with high accuracy is rarely available in practice.

Most studies in the field of co-operation of electricity and gas systems with wind uncertainty have only focused on traditional stochastic method (SM) [9], [10] and [11]. To obtain a reasonably high guarantee requires a large number

of wind scenario samples, which results in a problem that is computationally intensive.

Robust model (RM): A considerable amount of literature has been published on the RM [14], [15] and [16]. With respect to SM, this one does not rely on the number of scenarios, instead, it considers bounded intervals for the uncertain parameters [14]. However, the main disadvantage of RM is that the robustness region or horizon of the uncertainty is fixed before solving the problem. In fact, the goal of the decision maker is minimizing the objective function, e.g., operation cost.

In [15] and [16] the co-optimization scheduling of electricity and natural gas systems with the RM. However, co-optimization of the horizon of the uncertainty and operation cost have not been measured by these references.

Information-gap decision theory (IGDT) model: Unlike the RM, the objective of the IGDT model is maximizing the region or horizon of the uncertainty while satisfying a predetermined objective function, e.g., operation cost, which is major disadvantage for this model [17].

Accordingly, with the robust and IGDT models could not reach an optimal horizon of the uncertainty and operation cost, simultaneously. Noted that, to the best of authors' knowledge, the previous studies in the area have not addressed this issue yet [17], [18] and [19].

In the literature on coordination of interdependent natural gas and electricity systems, the relative importance of IGDT model in uncertainty model has been subject to considerable discussion [18] and [19]. But, the co-optimization of horizon of the uncertainty and total cost, simultaneously, has not been investigated by these references.

Fuzzy IGDT model: To overcome above models problems and in order to address second question, in this study propose a new IGDT method based on the fuzzy model [20] called fuzzy IGDT (F-IGDT) model. The F-IGDT model can co-optimize both uncertainty horizon and operation cost, simultaneously. Also, unlike the SM, this model does not rely on the number of scenarios and it is tractable and does not increase the complexity of the existing problem, and hence, the problem sustains a reasonable size.

B. Contribution

In this paper presents a continuous-time model for co-operation of integrated electricity-natural gas system to better capture the ramping capability of the NGFGs and EDRPs to track the continuous-time WPG and load changes.

The literature on the continuous-time model can be reached in [21], [22], [23] and [24]. However, the model proposed in this paper differs from the above references in five aspects:

- The continuous-time models for natural gas system and electricity demand response program have not been presented.
- The network security constraints have not been considered by [21], [22], [23] and [24].
- The wind uncertainty has not been investigated in [21], [22], [23] and [24]. The problem models in these references are deterministic.
- Finally, no research has been found that proposed fuzzy IGDT model for wind uncertainty management and co-optimize both uncertainty horizon and operation cost, simultaneously.

The major contributions of this work can be summarized as:

(i) Developing a CTM to co-operation of fast-response resources, i.e., the NGFGs, and EDRPs to capture the sub-hourly ramping capability of these resources to cover the sub-hourly variations of WEGs. Similarly, this study indicates that the CTM would modify the day-ahead commitment and schedule of NGFGs, and would utilize the EDRPs in such a way that the composition of the NGFGs and EDRPs can be better reduced natural gas consumer for the NGFGs.

(ii) The main aim of this study is to propose uncertainty model that can co-optimize of horizon of the uncertainty and objective function, simultaneously. So, in this study, a new fuzzy IGDT model to manage wind uncertainty has been proposed which can co-optimize both uncertainty horizon and operation cost, simultaneously. Also, in this study performance of proposed fuzzy IGDT model is compared with other previous uncertainty models, i.e., SM, RM and IGDT. Simulation results shows the efficiency of the fuzzy IGDT model.

II. Bernstein Polynomials

Before to begin this process, different approaches have existed that can be used to address the continuous-time model of a function or a data set [21] and [22]. In this paper, the Bernstein polynomial (BP) approach, among different approaches, has been chosen to model a function or a data set in continuous-time model. A major advantage of the BP approach is that when the piecewise approximation of a set of data points are implemented in problem, the Bernstein polynomials a bold feature of is that they can be utilized to more easily impose smoothness conditions not only at the break points but also inside the interval of interest, working only on the coefficients of the Bernstein spline expansion. Criteria for selecting the BP approach was as follows:

(i) To approximate the continuous-time trajectory (space) of a data set it can be utilized to more easily impose smoothness conditions not only at the break points but also inside the interval of interest, working only on the coefficients of the Bernstein spline expansion.

(ii) Implement this approach is simple.

(iii) The accuracy of BP approach is adjustable.

(iv) This approach can be calculated very quickly on a computer [21].

The BP of degree Q plays a vital role in the continuous-time model. Thus, the procedures of the BP approach are explained in detail as follows:

At first, the $Q+1$ Bernstein basis polynomials of degree $Q$are defined as:

$$B_{q,Q}^{t} = \binom{Q}{q} t^{q}(1-t)^{Q-q} \tag{1}$$

where $\binom{Q}{q}$ is a binomial coefficient.

To model a function, i.e., x_t, for time period T, in continuous-time model, the following steps should be imple-

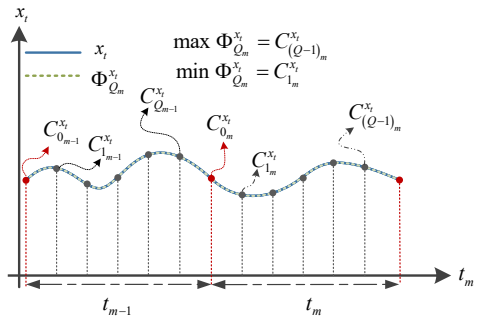

Fig. 1: The Bernstein coefficients for x_t.

mented:

(i) The time period T is divided into M intervals, i.e., $T_m = [t_m, t_{m+1}) \rightarrow T = \cup_{m=1}^{M} T_m$, length of each interval is $T_m = t_{m+1} - t_m$.

(ii) The BP operator $\Phi^{x_t}_{Q_m}$ is implemented on function x_t at each interval $[t_m, t_{m+1})$ and maps it into a Qth-order polynomial.

$$\Phi^{x_t}_{Q_m} = \sum_{q_m=0}^{Q_m} C^{x_t}_{q_m} B^{t-t_m}_{q_m,Q_m}, \quad t \in [t_m, t_{m+1}) \tag{2}$$

Where, the coefficients $C^{x_t}_{q_m}$ are called Bernstein coefficients or control points.

To represent the equation (2) in the matrix form, which is easy to implement, it can be divided into the product of Bernstein coefficients and Bernstein basis functions for $m = 1, \ldots, M; q = 0, \ldots, Q$ as follows:

$$\Phi^{x_t}_{Q_m} = \begin{bmatrix} C^{x_t}_{0_m} & C^{x_t}_{1_m} & \cdots & C^{x_t}_{Q_m} \end{bmatrix} \begin{bmatrix} B^{t-t_m}_{0_m,Q_m} \\ B^{t-t_m}_{1_m,Q_m} \\ \vdots \\ B^{t-t_m}_{Q_m,Q_m} \end{bmatrix} = \vec{C}^{x_t}_{Q_m} \vec{B}^{t-t_m}_{q_m,Q_m} \tag{3}$$

The other useful properties of BPs are as follows:

(i) Error approximation reduces once the order $Q_m$for $\Phi^{x_t}_{Q_m}$ is increased, i.e., $\lim_{Q_m \rightarrow \infty} \Phi^{x_t}_{Q_m} = x_t$. (ii) The derivative of $\Phi^{x_t}_{Q_m}$ is written as a summation of two polynomials of lower degree $(Q-1)_m$.

$$\dot{\Phi}^{x_t}_{(Q-1)_m} = Q_m \sum_{q_m=0}^{(Q-1)_m} \left(C^{x_t}_{q_m} - C^{x_t}_{(q-1)_m} \right) B^{t}_{q_m,(Q-1)_m} \tag{4}$$

(iii) Convex hull property of $B^t_{q,Q}$ causes that coefficients of $\Phi^{x_t}_{Q_m}$ and $\dot{\Phi}^{x_t}_{(Q_m-1)}$ are limited between their max and min coefficients (as shown in Fig.1).

$$\min \left\{ C^{x_t}_{q_m} \right\} \leq \vec{C}^{x_t}_{Q_m} \leq \max \left\{ C^{x_t}_{q_m} \right\} \tag{5}$$

This property significantly helps later, when max and min limit on a variable is driven.

$$\overbrace{\left(\frac{C^{x_t}_{q_m} - C^{x_t}_{(q-1)_m}}{Q_m} \right)}^{\min} \leq \vec{C}^{x_t}_{Q_m} - \vec{C}^{x_t}_{(Q-1)_m} \leq \overbrace{\left(\frac{C^{x_t}_{q_m} - C^{x_t}_{(q-1)_m}}{Q_m} \right)}^{\max} \tag{6}$$

Also, this property helps later, when max and min ramping constraints are driven.

(iv) In order to maintain continuity across first and end points of function x_t, it is sufficient to enforce that the control points match at the first and end points.

$$C^{x_t}_{0_m} = C^{x_t}_{Q_{m-1}} \tag{7}$$

Besides, the differential of $\Phi^{x_t}_{Q_m}$ should also be continuous.

$$C^{x_t}_{1_m} - C^{x_t}_{0_m} = C^{x_t}_{Q_{m-1}} - C^{x_t}_{(Q-1)_{m-1}} \tag{8}$$

These properties significantly help later to maintain generation and ramping continuity for GUs.

(v) The other important property of the BP operator that is used to represent objective function, which is presented by:

$$\int_{t_m}^{t_{m+1}} \Phi^{x_t}_{Q_m} = \int_{t_m}^{t_{m+1}} \left(\vec{C}^{x_t}_{Q_m} \vec{B}^{t}_{Q_m} \right) dt = \vec{C}^{x_t}_{Q_m} \int_{t_m}^{t_{m+1}} \vec{B}^{t}_{Q_m} dt$$
$$\frac{\vec{C}^{x_t}_{Q_m} \cdot \vec{1}_{Q_m}}{Q_m + 1} = \frac{\sum_{q_m=0}^{Q_m} C^{x_t}_{q_m,Q_m}}{Q_m + 1} \tag{9}$$

In (9) vector $\vec{C}^{x_t}_{Q_m}$ is constant parameter in definite integral and the definite integral, i.e., $\int_{t_m}^{t_{m+1}} \vec{B}^{t}_{Q_m} dt$, from an initial position t_m to a final position t_{m+1} is $\vec{1}_{Q_m}$ which is a $Q_m \times 1$-dimensional unit vector for given Q_m. These properties significantly help later to compute objective function.

III. CONTINUOUS-TIME MODELING

The original optimization problem is a kind of continuous-time co-operation of electricity and natural gas systems that minimizes the total cost (TC) of electric power system over the scheduling period subject to constraints (11)-(43).

$$\overbrace{\left(\begin{array}{l} \sum_g \left(\int_T \left(c_g \cdot G_{gt} + c^{su}_g \cdot y_{gt} \right) dt \right) \\ + \sum_n \left(\int_T \left(c_n \cdot \left(\Delta D^{+}_{nt} + \Delta D^{-}_{nt} \right) \right) dt \right) \end{array} \right)}^{\min \text{TC}} \tag{10}$$

The TC (10) includes: (i) the continuous-time generation and startup costs of generating units (GUs) (first and second terms), and (ii) the continuous-time cost of EDRP.

In the following, the continuous-time formulation of electricity and natural gas constraints has been discussed.

A. Continuous-time Constraints of Electricity Network

The constraints of the electricity network have been modeled by a number of continuous-time equations as follow:

$$\underline{G}_g I_{gt} \leq G_{gt} \leq \overline{G}_g I_{gt} \tag{11}$$

$$\underline{\dot{G}}_g I_{gt} \leq \frac{dG_{gt}}{dt} = \dot{G}_{gt} \leq \overline{\dot{G}}_g I_{gt} \tag{12}$$

$$\int_t^{t-UT_g+1} I_{gt'} dt' \leq UT_g y_{gt} \tag{13}$$

$$\int_t^{t-DT_g+1} \left(1 - I_{gt'} \right) dt' \leq DT_g z_{gt} \tag{14}$$

$$y_{gt} - z_{gt} = I_{gt} - I_{gt-1} \tag{15}$$

$$f_{kt} = b_{nm} \cdot \left(\theta_{nt} - \theta_{mt} \right) \tag{16}$$

$$-\overline{f}_k \leq f_{kt} \leq \overline{f}_k \tag{17}$$

$$D_{nt} = D_{nt}^{f} + \Delta D_{nt}^{+} - \Delta D_{nt}^{-} \tag{18}$$

$$0 \le \Delta D_{nt}^{+} / \Delta D_{nt}^{-} \le \Delta \Phi^{\pm} \tag{19}$$

$$\underline{\dot{D}}_{n} \le \frac{dD_{nt}}{dt} = \dot{D}_{nt} \le \overline{\dot{D}}_{n} \tag{20}$$

$$0 \le \int_{T} \left(\Delta D_{nt}^{+} - \Delta D_{nt}^{-} \right) dt \le \Delta E_{n} \tag{21}$$

$$\sum_{g(n)} G_{gt} + \sum_{w(n)} \bar{W}_{wt} - \sum_{k(n,m)} f_{kt} + \sum_{k(m,n)} f_{kt} = D_{nt} \tag{22}$$

$$G_{g,t=0} = G_{g}^{0}, D_{n,t=0} = D_{n}^{0} \tag{23}$$

Equation (11) imposes the continuous-time lower and upper limits on power generation for GUs. Continuous-time up and down ramping route constraints are shown by Equation (12). Equations (13) and (14) are continuous-time minimum ON/OFF time constraints for each GUs.

Equation (15) indicates ON or OFF states for each GU, e.g., if $y_{gt} = 1$ thenz_{gt} is 0, in this condition GU is turned on, and if $y_{gt} = 0$ then z_{gt} is 1, in this condition GU is turned off.

The DC power flow for each transmission line is enforced by Equation (16). Equation (17) sets maximum transmission line power flows. Equation (18) denotes the flexible demands for EDRP. In Equation (18), D_{nt}^{f} represents the fixed demand, and $\Delta D_{nt}^{+} / \Delta D_{nt}^{-}$ represents the increase/decrease value for the fixed demand. The increase/decrease value for the flexible demand is limited by Equation (19). Equation (20) implements the continuous-time ramp up/down limits of the flexible demands. The continuous-time ramp up/down denote how a flexible demand can decrease or increase its consumption. Noted that, the associated continuous-time ramp up/down of the flexible demands are determined by means of derivation of the demand consumption routes with respect to the time. Equation (21) imposes the limit on the adequate energy changes through the continuous-time demand responses. Equation (22) enforce continuous-time power balance at each bus. Initial values of the state routes are enforced in (23), where G_{g}^{0} and D_{n}^{0} are vectors of constant initial values.

B. Continuous-time Natural Gas Constraints

The natural gas system has been formulated with a number of continuous-time equations as follow:

$$\rho_{it} = \overline{\rho}_{i} \tag{24}$$

$$\underline{\rho}_{i} \le \rho_{it} \le \overline{\rho}_{i} \tag{25}$$

$$\sum_{\ell} \left(\varphi_{\ell p} \cdot f_{\ell pt} + \gamma_{\ell p} \cdot \nu_{\ell pt} \right) = \Theta_{p} \left(\rho_{it} - \rho_{jt} \right) \tag{26}$$

$$\nu_{\ell pt} \cdot \underline{f}_{\ell p} \le f_{\ell pt} \le \nu_{\ell pt} \cdot \overline{f}_{\ell p} \tag{27}$$

$$f_{pt} = \sum_{\ell} f_{\ell pt} \tag{28}$$

$$\sum_{\ell} \nu_{\ell pt} \le 1 \tag{29}$$

$$\underline{g}_{i} \le g_{it} \le \overline{g}_{i} \tag{30}$$

$$L_{it} = L_{it}^{e} + L_{it}^{n} \tag{31}$$

$$\sum_{\ell} \left(\varphi_{\ell p} \cdot f_{\ell pt} + \gamma_{\ell p} \cdot \nu_{\ell pt} \right) \ge \Theta_{p} \left(\rho_{it} - \rho_{jt} \right), \quad \forall p \in \Omega_{c} \tag{32}$$

$$f_{pt} \ge 0, \quad p \in \Omega_{c} \tag{33}$$

$$\rho_{it} \le \lambda_{p} \rho_{jt}, \ p \in \Omega_{c} \tag{34}$$

$$\frac{dE_{st}}{dt} = S_{st}^{in} - S_{st}^{out} \tag{35}$$

$$\underline{E}_{s} \le E_{st} \le \overline{E}_{s} \tag{36}$$

$$\underline{S}_{s}^{in} \le S_{st}^{in} \le \overline{S}_{s}^{in} \tag{37}$$

$$\underline{S}_{s}^{out} \le S_{st}^{out} \le \overline{S}_{s}^{out} \tag{38}$$

$$\underline{\dot{S}}_{s}^{out} \le \frac{dS_{st}^{out}}{dt} = \dot{S}_{st}^{out} \le \overline{\dot{S}}_{s}^{out} \tag{39}$$

$$\underline{\dot{S}}_{s}^{in} \le \frac{dS_{st}^{in}}{dt} = \dot{S}_{st}^{in} \le \overline{\dot{S}}_{s}^{in} \tag{40}$$

$$L_{lt}^{e} = \alpha + \beta G_{gt} + \gamma G_{gt}^{2} \tag{41}$$

$$\sum_{s(i)} \left(S_{st}^{in} - S_{st}^{out} \right) + \sum_{p(i,j)} f_{ij} - \sum_{p(j,i)} f_{ji} + \sum_{G(i)} g_{it} = L_{lt} \tag{42}$$

$$g_{i,t=0} = \tilde{g}_{i}, S_{s,t=0}^{out} = \tilde{S}_{s}^{out}, S_{s,t=0}^{in} = \tilde{S}_{s}^{in}, E_{s,t=0} = \tilde{E}_{s} \tag{43}$$

There are certain similarities between electricity and natural gas transmission systems. Both systems are planned to supply end users through their respective transmission system. The natural gas transmission system is included of transmission pipelines (high pressure), distribution pipelines (low pressure), natural gas customers, natural gas wells, and storage facilities. Similar to electricity transmission system, the natural gas transmission system can be represented by its steady-state and dynamic characteristics [23]. The steady-state mathematical model included of a group of linear equations is presented in this study. From the mathematical viewpoint, the steady-state natural gas problem is like electricity transmission system problem but which will determine the state variables including flow rates and nodal pressures in different pipelines based on the known injection values of natural gas load and supply.

Equation (24) shows that at the source nodes, the square of natural gas pressure is at the maximum value. Equation (25) enforces the lower and upper limits on the square of natural gas pressure at the demand nodes. The modeling of the natural gas flow through a pipeline from node i to node j without (with) compressor is a nonlinear equation, i.e., the Weymouth equation. Accordingly, in this paper a piecewise linear equation for natural gas flow over a pipeline has been developed with the aim of decreasing computational burden [10].

Natural gas is delivered to (non-) electric loads via gas pipelines. The gas pipelines comprise active pipeline (with compressor) and passive pipeline (without compressor). Actually, in active pipelines the compressors would increase the gas pressure difference between the corresponding nodes to enhance the transmission capacity. Natural gas flows in

pipelines are dependent on factors such as the operating temperatures, pressures, diameter of pipelines and length, altitude change over the transmission path, the roughness of pipelines and type of natural gas.

The natural gas flow through a pipeline from node i to node j without compressor is formulated linearly through Equations (26) – (29). Equation (26) relates to the linear Weymouth equation for the pipeline without compressor. In this equation, Θ_p is a parameter which depends on the pipeline features, length, temperature, natural gas compositions, friction and diameter. Equation (27) imposes min/max limits on the piecewise linear segments; Equation (28) calculates the total gas flow over the pipeline. Equation (29) lets only one segment to be active.

Detail of the linear Weymouth equation are given by Appendix A. Natural gas supplies have modeled as positive gas injections at related nodes. The lower and upper limits of gas supplier at each period is modelled by Equation (30). Natural gas consumers are classified into industrial loads (electric loads), (commercial) residential loads (non-electric loads) with different urgencies. In fact, the NGFGs are the largest industrial loads (electric loads) of NGSs which links the natural gas system with the electric transmission systems. The urgency of industrial loads is lower than that of residential loads (non-electric loads) in the natural gas scheduling horizon. Equation (31) models the natural gas load for non-electric load, i.e., L^n_{it}, and electric load, i.e., L^e_{it}. The gas flow in pipeline with gas compressor is specified by Equation (32).

Equation (33), indicates that the pipeline with gas compressor generally has a predefined continuous-time gas flow direction. Furthermore, terminal nodal square of pressures of the pipeline with gas compressor is constrained via compressor factor as shown in Equation (34). The state of charge (SOC) of natural gas storage units (NGSUs) is controlled using the continuous-time differential Equation (35) during the scheduling period.

The limitations on the gas storage capacity, natural gas inflow/outflow, and inflow/outflow ramping routes over T for each NGSUs, are imposed by Equations (36)–(40), respectively, wherein the min and max limits of the routes have been denoted by the underlined and overlined constant terms, respectively. Equation (41) links natural gas and electricity systems. This equation indicate that the natural gas required by each NGFGs depends on its continuous-time generation dispatch. A continuous-time nodal balance constraint (42) indicates that the natural gas flow injected at a node is equal to the gas flowing out of the node.

The starting (initial) values for the state routes are stated in (43) wherein $\tilde{g}_i$, $\tilde{S}^{out}_s$, $\tilde{S}^{in}_s$, and $\tilde{E}_s$ are constant initial values of each decision variable.

IV. Modeling Continuous-Time Equations In Bernstein Function Space

The proposed continuous-time problem (10)-(43) is optimization problem with infinite-dimensional decision space that is computationally intractable. Accordingly, in this section a function space-based solution method has been proposed for the proposed continuous-time problem (10)-(43). The proposed solution method is based on reducing the dimensionality of the continuous-time decision and parameter trajectories by modeling them in a finite-order function space spanned by the BP approach.

A. Objective Function

The main advantage of using BP approximate is that they can be calculated very quickly on a computer. According to (9), the continuous time form for objective function (10) can be written as follows:

$$\overbrace{\left(\begin{array}{l}\sum\limits_{g}\left(\int\limits_{T}\left(c_g\cdot\vec{C}^{G_{gt}}_{Q_m}\cdot\vec{B}^{t}_{Q_m}+c^{su}_{g}\cdot y_{gt}\right)dt\right)\\+\sum\limits_{n}\left(\int\limits_{T}\left(c_n\cdot\left(\vec{C}^{\Delta D^{+}_{nt}}_{Q_m}\cdot\vec{B}^{t}_{Q_m}+\vec{C}^{\Delta D^{-}_{nt}}_{Q_m}\cdot\vec{B}^{t}_{Q_m}\right)\right)dt\right)\end{array}\right)}^{\min} \tag{44}$$

Substituting the Bernstein representations of $\left\{G_{gt},\Delta D^{+}_{nt},\Delta D^{-}_{nt}\right\}$, according to (3), i.e., $\left\{\vec{C}^{G_{gt}}_{Q_m}\cdot\vec{B}^{t}_{Q_m},\vec{C}^{\Delta D^{+}_{nt}}_{Q_m}\cdot\vec{B}^{t}_{Q_m}+\vec{C}^{\Delta D^{-}_{nt}}_{Q_m}\cdot\vec{B}^{t}_{Q_m}\right\}$, in (10), and integrating the right-hand-sides over T , the linear generation and startup costs of generating units (GUs), and cost of EDRP over T in terms of the Bernstein basis function are calculated.

$$\overbrace{\left(\begin{array}{l}\sum\limits_{g}\sum\limits_{t}\left(c_g\cdot\sum\limits_{m}^{M}\frac{\sum\limits_{q_m}^{Q}C^{G_{gt}}_{q_m,Q_m}}{Q_m+1}+c^{su}_{g}\cdot y_{gt}\right)\\+\sum\limits_{n}\sum\limits_{t}c_n\cdot\sum\limits_{m}^{M}\frac{\sum\limits_{q_m}^{Q_m}\left(C^{\Delta D^{+}_{nt}}_{q_m,Q_m}+C^{\Delta D^{-}_{nt}}_{q_m,Q_m}\right)}{Q_m+1}\end{array}\right)}^{\min\Theta} \tag{45}$$

Equation (45) is the continuous time form of objective function (10) in terms of the Bernstein representation. The following section presents, the continuous-time model of electric power and natural gas constraints base on the BP operator have been presented.

B. Electric and Non-Electric Loads and Wind Profiles

The electric load, non-electric load and wind power profiles are similar to Fig.1. Accordingly, these profiles can be modelled by the vector of Bernstein basis functions of degree Q in hour t_m as follows:

$$\begin{cases}\Phi^{\Omega}_{Q_m}=\vec{C}^{\Omega}_{Q_m}\vec{B}^{t-t_m}_{Q_m},\\ \forall t\in[t_m,t_{m+1}),\ \Omega\in\left\{D_{nt},L^n_{it},W_{f,wt}\right\}\end{cases} \tag{46}$$

where $\vec{C}^{\Omega}_{Q_m}$ is Bernstein basis vector that each element of this vector is weighted via the values of electric load, non-electric load and wind power at the hour t_m, like to Fig.1.

C. Electricity Network Constraints

$$\underline{G}_g I_{gt} \leq \vec{C}^{G_{gt}}_{Q_m} \leq \overline{G}_g I_{gt} \tag{47}$$

$$\frac{\dot{\underline{G}}_g I_{gt}}{Q_m} \leq \vec{C}^{G_{gt}}_{Q_m} - \vec{C}^{G_{gt}}_{(Q_m-1)} \leq \frac{\dot{\overline{G}}_g I_{gt}}{Q_m} \tag{48}$$

$$\sum_{t'=t-UT_g+1}^{t} I_{gt'} \leq UT_g y_{gt} \tag{49}$$

$$\sum_{t'=t-DT_g+1}^{t} (1 - I_{gt'}) \leq DT_g z_{gt} \tag{50}$$

$$y_{gt} - z_{gt} = I_{gt} - I_{gt-1} \tag{51}$$

$$\vec{C}^{f_{kt}}_{Q_m} = b_{nm} \cdot \left(\vec{C}^{\theta_{nt}}_{Q_m} - \vec{C}^{\theta_{mt}}_{Q_m} \right) \tag{52}$$

$$-\overline{f}_k \leq \vec{C}^{f_{kt}}_{Q_m} \leq \overline{f}_k \tag{53}$$

$$\vec{C}^{D_{nt}}_{Q_m} = \vec{C}^{D^f_{nt}}_{Q_m} + \left(\vec{C}^{\Delta D^+_{nt}}_{Q_m} - \vec{C}^{\Delta D^-_{nt}}_{Q_m} \right) \tag{54}$$

$$0 \leq \vec{C}^{\Delta D^+_{nt}}_{Q_m} / \vec{C}^{\Delta D^-_{nt}}_{Q_m} \leq \Delta\Phi^{\pm} \tag{55}$$

$$\frac{\dot{\underline{D}}_n}{Q_m} \leq \vec{C}^{\dot{D}_{nt}}_{Q_m} - \vec{C}^{\dot{D}_{nt}}_{(Q-1)_m} \leq \frac{\dot{\overline{D}}_n}{Q_m} \tag{56}$$

$$\frac{\sum_{q_m}^{Q_m} \left(C^{\Delta D^+_{nt}}_{q_m} - C^{\Delta D^-_{nt}}_{q_m} \right)}{Q_m + 1} \leq \Delta E_n \tag{57}$$

$$\sum_{g(n)} \vec{C}^{G_{gt}}_{Q_m} + \sum_{w(n)} \vec{C}^{\bar{W}_{wt}}_{Q_m} - \sum_{k(n,m)} \vec{C}^{f_{kt}}_{Q_m} + \sum_{k(m,n)} \vec{C}^{f_{kt}}_{Q_m} = \vec{C}^{D_{nt}}_{Q_m} \tag{58}$$

$$\vec{C}^{G_{g,t=0}}_{Q_m} = \vec{C}^{G^0_g}_{Q_m}, \vec{C}^{D_{n,t=0}}_{Q_m} = \vec{C}^{D^0_n}_{Q_m} \tag{59}$$

According to (5), in (47), the coefficient of the Bernstein representations of G_{gt}, i.e., $\vec{C}^{G_{gt}}_{Q_m}$, is limited between their max and min coefficients. Similarly, according to (6) the continuous-time ramping trajectories of GUs, i.e., (12), can be driven by (48). In fact, Equation (48) imposes enforce a limitation on the continuous-time GU ramping model. In this study, supposed that ON or OFF states for each GU are happen only for hourly discrete time. For example, a GU can be turned on or turned off only in first or end of an hour. Therefore, the continuous time definite integral in (13) and (14) can be converted into discrete time summation in (49) and (50). Noted that, the continuous time and discrete time model of Equation (15) is similar. Thus, Equations (15) and (51) are alike and indicate ON or OFF states for each GU. The continuous-time model of Equation (16) can be formulated by Equation (52). Substituting the Bernstein representations of $\{f_{kt}, \theta_{nt}, \theta_{mt}\}$, i.e., $\left\{ \vec{C}^{f_{kt}}_{Q_m} \cdot \vec{B}^{t-t_m}_{Q_m}, \vec{C}^{\theta_{nt}}_{Q_m} \cdot \vec{B}^{t-t_m}_{Q_m}, \vec{C}^{\theta_{mt}}_{Q_m} \cdot \vec{B}^{t-t_m}_{Q_m} \right\}$, in (16) and removing $\vec{B}^{t-t_m}_{Q_m}$ from both sides of the Equation (16), we have Equation (52). According to (5), in Equation (53) the $\vec{C}^{f_{kt}}_{Q_m}$ can be limited between max and min Bernstein coefficients, i.e., $-\bar{f}_k / \bar{f}_k$. The continuous time form of Equation (54) similar to (52) can be represented by vector of Bernstein basis functions of degree Q. Equations (55)-(56) are Equations (18)-(20) in terms of the Bernstein representation. According to (9), Equation (21) can be converted to (57). According to (2) and (46), Substituting the Bernstein models of GUs, wind power generation, line flow and electrical demand in the continuous time power balance Equation (22), and eliminating $\vec{B}^{t-t_m}_{Q_m}$ from both sides, we have Equation (58). Equation (59) are vectors of constant initial values for Bernstein coefficients at time 0.

D. Natural Gas Constraints

$$\vec{C}^{\rho_{it}}_{Q_m} = \vec{C}^{\bar{\rho}_i}_{Q_m} \tag{60}$$

$$\underline{\rho}_i \leq \vec{C}^{\rho_{it}}_{Q_m} \leq \overline{\rho}_i \tag{61}$$

$$\sum_{\ell} \left(\varphi_{\ell p} \cdot \vec{C}^{f_{\ell pt}}_{Q_m} + \gamma_{\ell p} \cdot \vec{C}^{\nu_{\ell pt}}_{Q_m} \right) = \Theta_p \left(\vec{C}^{\rho_{it}}_{Q_m} - \vec{C}^{\rho_{jt}}_{Q_m} \right) \tag{62}$$

$$\vec{C}^{\nu_{\ell pt}}_{Q_m} \cdot \underline{f}_{\ell p} \leq \vec{C}^{f_{\ell pt}}_{Q_m} \leq \vec{C}^{\nu_{\ell pt}}_{Q_m} \cdot \overline{f}_{\ell p} \tag{63}$$

$$\vec{C}^{f_{\ell pt}}_{Q_m} = \sum_{\ell} \vec{C}^{f_{\ell pt}}_{Q_m} \tag{64}$$

$$\sum_{\ell} \vec{C}^{\nu_{\ell pt}}_{Q_m} \leq 1 \tag{65}$$

$$\underline{g}_i \leq \vec{C}^{g_{it}}_{Q_m} \leq \overline{g}_i \tag{66}$$

$$\vec{C}^{L_{it}}_{Q_m} = \vec{C}^{L^e_{it}}_{Q_m} + \vec{C}^{L^n_{it}}_{Q_m} \tag{67}$$

$$\sum_{\ell} \left(\varphi_{\ell p} \cdot \vec{C}^{f_{\ell pt}}_{Q_m} + \gamma_{\ell p} \cdot \vec{C}^{\nu_{\ell pt}}_{Q_m} \right) \geq \Theta_p \left(\vec{C}^{\rho_{it}}_{Q_m} - \vec{C}^{\rho_{jt}}_{Q_m} \right), \forall p \in \Omega_c \tag{68}$$

$$\vec{C}^{f_{pt}}_{Q_m} \geq 0, \quad p \in \Omega_c \tag{69}$$

$$\vec{C}^{\rho_{it}}_{Q_m} \leq \lambda_p \vec{C}^{\rho_{jt}}_{Q_m}, \ p \in \Omega_c \tag{70}$$

$$Q_m \left(\vec{C}^{E_{st}}_{Q_m} - \vec{C}^{E_{st}}_{(Q-1)_m} \right) = \vec{C}^{S^{in}_{st}}_{Q_m} - \vec{C}^{S^{out}_{st}}_{Q_m} \tag{71}$$

$$\underline{E}_s \leq \vec{C}^{E_{st}}_{Q_m} \leq \overline{E}_s \tag{72}$$

$$\underline{S}^{in}_s \leq \vec{C}^{S^{in}_{st}}_{Q_m} \leq \overline{S}^{in}_s \tag{73}$$

$$\underline{S}^{out}_s \leq \vec{C}^{S^{out}_{st}}_{Q_m} \leq \overline{S}^{out}_s \tag{74}$$

$$\frac{\dot{\underline{S}}^{out}_s}{Q_m} \leq \vec{C}^{S^{out}_{st}}_{Q_m} - \vec{C}^{S^{out}_{st}}_{(Q-1)_m} \leq \frac{\dot{\overline{S}}^{out}_s}{Q_m} \tag{75}$$

$$\frac{\dot{\underline{S}}^{in}_s}{Q_m} \leq \vec{C}^{S^{out}_{st}}_{Q_m} - \vec{C}^{S^{out}_{st}}_{(Q-1)_m} \leq \frac{\dot{\overline{S}}^{in}_s}{Q_m} \tag{76}$$

$$\vec{C}^{L^e_{lt}}_{Q_m} = \alpha + \beta \vec{C}^{G_{gt}}_{Q_m} + \gamma \vec{C}^{G^2_{gt}}_{Q_m} \tag{77}$$

$$\sum_{s(i)} \left(\vec{C}^{S^{in}_{st}}_{Q_m} - \vec{C}^{S^{out}_{st}}_{Q_m} \right) + \sum_{p(i,j)} \vec{C}^{f_{ij}}_{Q_m} - \sum_{p(j,i)} \vec{C}^{f_{ij}}_{Q_m} + \sum_{G(i)} \vec{C}^{g_{it}}_{Q_m} = \vec{C}^{L_{lt}}_{Q_m} \tag{78}$$

$$\vec{C}^{g_{i,t=0}}_{Q_m} = \vec{C}^{\tilde{g}_i}_{Q_m}, \vec{C}^{S^{out}_{s,t=0}}_{Q_m} = \vec{C}^{\tilde{S}^{out}_s}_{Q_m}, \vec{C}^{S^{in}_{s,t=0}}_{Q_m} = \vec{C}^{\tilde{S}^{in}_s}_{Q_m}, \vec{C}^{E_{s,t=0}}_{Q_m} = \vec{C}^{\tilde{E}_s}_{Q_m} \tag{79}$$

The converting equations of natural gas, i.e., (24)-(43), to the Bernstein function space are similar to Equations (11)-(23). Therefore, we utilize similar approach to convert Equations

(24)-(43) in terms of Bernstein function space. Equations (60) – (79) mimic (24) – (43) that defined in terms of Bernstein function space.

V. Fuzzy IGDT Method for Uncertainty Handling

A. IGDT Method

As mentioned, the core of the proposed fuzzy IGDT model is the IGDT approach. Accordingly, before describing the proposed approach, it is noted that there are two strategies to handle uncertainty by the IGDT as follows:
(i) Risk-averse (RA) strategy: The main goal of this strategy is to provide a conservative decision that increases the robustness of proposed optimization problem against WEG uncertainty.
(ii) Opportunity seeker (OS) strategy: In this strategy, the decision maker (DM) uses the uncertainty to decrease the total costs. In contrast to the RA strategy, in this strategy the WEG uncertainty is a favorite occurrence and it is related with higher WEG than the forecasted ones.
The optimization framework for the RA and OS strategies can be formulated as follows:

$$\max \pm\lambda \tag{80}$$

$$W_{wt} = (1 \mp \lambda) \cdot \bar{W}_{wt} \tag{81}$$

$$\Theta \leq \overbrace{\Theta_b(1 \pm \sigma_\Omega)}^{\Lambda_\Omega}, \quad \Omega \in \{r, o\} \tag{82}$$

$$(47) - (79) \tag{83}$$

In these strategies, at first the DM specifies the base cost $\Lambda_\Omega, \forall\Omega \in \{r, o\}$ for both strategies, then, it maximizes the objective function (80) to maximize the radius of WEG uncertainty meanwhile satisfying Equations (81) – (83). Noted that, "+" and "–" in (80) – (83) refer to the RA and OS strategies, respectively. Equation (81) indicates the radius of the WEG uncertainty that can be deviated from its forecasted value. Equation (82) is called as the 'budget level limit', which keeps the TC, i.e., Θ, lower than a specified level $\Lambda_\Omega, \forall\Omega \in \{r, o\}$. Noted that, r and o in $\Omega \in \{r, o\}$ refer to RA and OS strategies, respectively. In Equation (82),σ_Ω is a positive parameter determined by the DM. It should be noted that, to the choice of specified level of operation cost value, i.e, Λ_Ω. At first, it is assumed that there is no uncertainty exists in the model so the radius of WEG uncertainty would become 0 and the hourly WEG would be the same as its predicted value. In this condition IGDT problem (80)-(83) is solved then the base total cost find, i.e.,Θ_b . Then based on parameter σ_Ω in $(1 \pm \sigma_\Omega)$, the degree of greediness on further decreasing (improving) the value of base total cost due to the possible the radius of WEG uncertainty. Constraint (83) comprises by electric power constraints (47)-(59) and natural gas constraints (60)-(79).

B. Fuzzy IGDT Method

Recently, a considerable literature has grown up around the uncertainty management with IGDT method. Generally, during the optimization process for IGDT method, the TC is fixed to upper limit of inequality constraint, i.e., the cost threshold $\Lambda_{r/o}$. Therefore, in this model, the decision makers cannot achieve an optimal value for the TC [17]. To solve this issue, in this section, a new IGDT model based on fuzzy approach has been proposed to achieve optimal values for the TC and the radius of WEG uncertainty, i.e., $\pm\lambda$. The fuzzy model are able to handle multi-objective functions simultaneously such as the TC, i.e., Θ, and the radius of WEG uncertainty, i.e., $\pm\lambda$. In order to optimize these objective functions simultaneously, each objective function should be characterized by fuzzy sets [20] which are typically represented by a membership function, μ, with lower and upper boundaries together with a strictly monotonically decreasing and continuous function for different objectives functions. A further study with more focus on fuzzy approach can be found in [20]. A membership function for the RA and OS strategies can be defined as follows:

$$\mu_r(\lambda) = \begin{cases} 1 & \lambda \geq \lambda^{\max} \\ \dfrac{\lambda - \lambda^{\min}}{\lambda^{\max} - \lambda^{\min}} & \lambda^{\min} \leq \lambda \leq \lambda^{\max} \\ 0 & \lambda \leq \lambda^{\min} \end{cases} \tag{84}$$

$$\mu_o(\lambda) = \begin{cases} 1 & \lambda \geq \lambda^{\max} \\ \dfrac{\lambda^{\max} - \lambda}{\lambda^{\max} - \lambda^{\min}} & \lambda^{\min} \leq \lambda \leq \lambda^{\max} \\ 0 & \lambda \leq \lambda^{\min} \end{cases} \tag{85}$$

$$\mu_{OF}(\Theta) = \begin{cases} 0 & \Theta \geq \Theta^{\max} \\ \dfrac{\Theta^{\max} - \Theta}{\Theta^{\max} - \Theta^{\min}} & \Theta^{\min} \leq \Theta \leq \Theta^{\max} \\ 1 & \Theta \leq \Theta^{\min} \end{cases} \tag{86}$$

In the above equations, $\lambda^{\max}/\Theta^{\max}$ and $\lambda^{\min}/\Theta^{\min}$ are the maximum and the minimum values of the objective functions, i.e., Θ and λ are evaluated through the single-objective optimization. Equations (84) and (85) calculate membership functions $\mu_r(\lambda)$ and $\mu_o(\lambda)$ for the RA and OS strategies, respectively. Similarly, Equation (86) calculates the membership function $\mu_{OF}(\Theta)$ for both strategies.

$$\max \beta_{r/o} \tag{87}$$

$$\begin{cases} \dfrac{\lambda - \lambda^{\min}}{\lambda^{\max} - \lambda^{\min}} \geq \beta_r \\ \dfrac{\lambda^{\max} - \lambda}{\lambda^{\max} - \lambda^{\min}} \geq \beta_o \end{cases} \tag{88}$$

$$\frac{\Theta^{\max} - \Theta}{\Theta^{\max} - \Theta^{\min}} \geq \beta_{r/o} \tag{89}$$

$$(47) - (79) \text{ and } (81) - (82) \tag{90}$$

Equation (87) - (90) indicates F-IGDT model for the RA and OS strategies. It should be noted that, r and o are the initials of the RA and OS strategies, respectively. Equation (87) maximizes the degree of "overall satisfaction", $\beta_{r/o}$, i.e., for all of the membership functions. Noted that, β_r

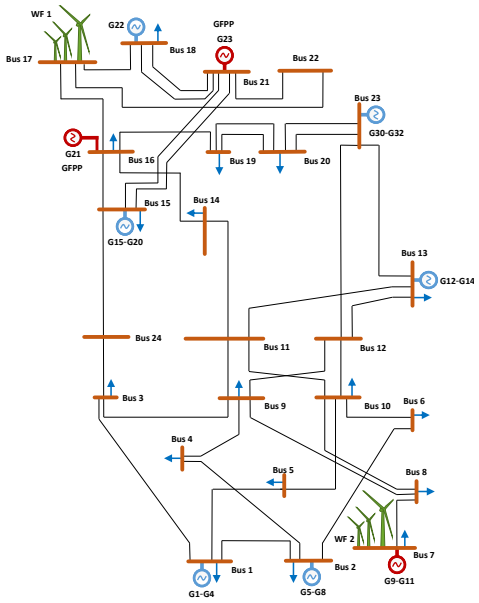

Fig. 2: Modified IEEE-RTS.

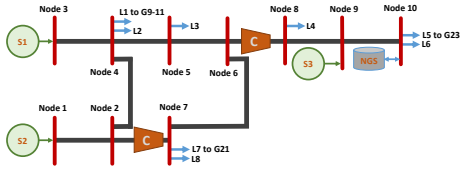

Fig. 3: Ten-node NGS.

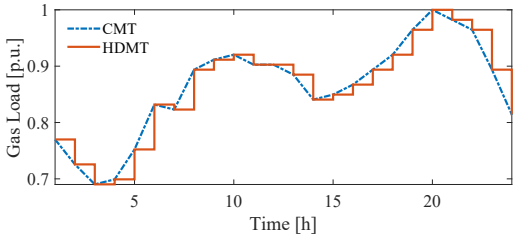

Fig. 4: The actual gas load curves for CTM and HDTM.

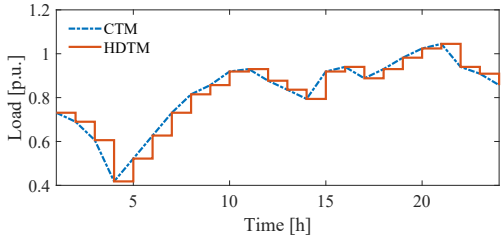

Fig. 5: The electricity load curves for CTM and HDTM.

and β_o indicates the level of satisfaction for the RA and OS, respectively. Equations (88) and (89), specify the linear membership function for each objective function in the RA and OS strategies. Equation (90) includes the equations (47)-(79) and (81)-(82) which are described before.

VI. Case Studies

This section presents numerical results for a case study based on a modified IEEE-RTS and IEEE 118 system. The proposed formulation with the CTM and HDTM have been solved by CPLEX 12.6.2 on a PC with Intel Core-i7 processor at 4.2 GHz and 16 GB of RAM.

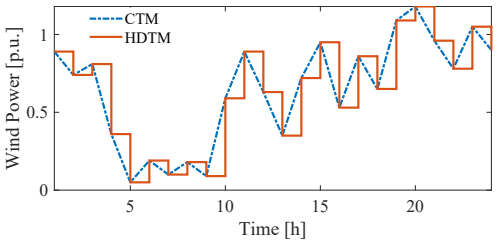

Fig. 6: The wind power curves for CTM and HDTM.

A. Modified IEEE-RTS

In this section, to demonstrate the performance of the proposed model, the modified IEEE-RTS [23] with a six-node natural gas system [24] has been implemented. As shown in Fig. 2, the modified IEEE-RTS includes 2 wind farms, 21 fossil units (blue color), 5 natural gas-fired units (red color), 38 transmission lines and 17 load buses. Two wind farms with the 250 MW and 550 MW capacities have been installed at buses 7 and 17, respectively. The ten-node natural gas system consists of 3 suppliers, 2 compressors, 1 natural gas storage (NGS), 8 natural gas loads, and 10 pipelines which has been shown by Fig. 3. In Fig. 3, L1, L5 and L7 are natural gas loads consumed by G9-10, G21 and G23, respectively. Similarly, L2, L3, L4, L6 and L8 represent other types of natural gas residential natural gas end-users. The other parameters of the natural gas system can be found in [24]. The BPs of degree 5 have been used to simulate the proposed CTM. The natural gas load, electricity load and wind power profiles for CTM and HDTM are shown in Figs. 4-6, respectively. For each case, the solution results of the CTM and HDTM have been compared.

1) Comparison Performance of F-IGDT and IGDT Models: Here, for the IGDT model, we set the budget limit as (for the RA strategy) and (for the OS strategy) to compare the performances of F-IGDT and IGDT models. The results of this comparison can be found in Tables I-IV. As mentioned before the main objective of the IGDT model is minimizing or maximizing λ value and in this model the TC value is considered as an inequality constraint in optimization process. Accordingly, the solution results, i.e., λ and TC values, for this model are very conservatism. To tackle the above shortage of the IGDT model, here, proposed an F-IGDT model to take both λ and TC values in objective function and obtain optimal values for them. For example, as can be seen in Table I, in the IGDT model and for RA strategy without NGS, when the λ value is 0.231 but for the F-IGDT model, TC and λ values are and 0.228, respectively. The results of the IGDT model show that the TC value is set to predefined value, i.e., and the λ value is in highest value, i.e., 0.231. Therefore, these values are very conservatism. But for F-IGDT model, the TC and λ values are considered in objective function with fuzzy technique, thus, they are less conservative in comparison to the IGDT model results. Furthermore, the F-IGDT model shows better performance than the IGDT model while it has the optimal value for the TC. On the other hand, the results of

this study indicate that the CTM or HDTM in (F-) IGDT model can affect the TC and λ values. Accordingly, it is apparent from Table I that the CTM for F-IGDT model has the positive effect on the TC and λ values, which can decrease the TC value and increase the λ value. For example, for the fuzzy RA, without NGS and EDRP, the TC and λ values for the HDTM are 94515.492 $ and 0.228, respectively. But, these values for the CTM are 80328.521 $ and 0.261, respectively. Similarly, for fuzzy OS, without NGS and EDRP, the TC and λ values for the HDTM are 72766.024 $ and 0.229, respectively, and these values for the CTM are 67768.371 $ and 0.117, respectively. The results, as shown in Table I, indicate that the CTM has better results in the F-IGDT model while it has decreased the TC and increased the λ value for both fuzzy RA and OS strategies.

2) Gas Consumption of NGFGs without (with) NGS: Gas consumption of five NGFGs, i.e., G9, G10, G11, G21 and G23, without (with) NGS constraints are shown in Tables III and IV. All NGFGs were most dispatched in power system operation because their generation costs are inexpensive and they have the highest ramping capability. Fossil units are placed at the second rank since they are the most expensive and have low ramping capability. Also, for the electrical power systems integrated with large-scale WEG, significant amounts of WEG cannot be absorbed due to low ramping capability. Accordingly, dispatching of NGFGs has enhanced the ramping capacity and consequently absorbing more WEGs. Hence, the fuel consumptions of five NGFGs is in the highest level once the NGS constraints are not considered. Nevertheless, as can be seen from Table IV, once the NGS constraints are incorporated for five NGFGs, the fuel consumptions of the five cheapest NGFGs are reduced since the NGS constraints have limited the supply of fuel. For this reason, the outputs of the five cheapest NGFGs are decreased and it has enforced the expensive fossil units to be committed. Moreover, Tables III and IV shows the fuel consumptions of the five cheapest NGFGs, for HDTM and CTM. It is seen from these tables that the fuel consumptions of NGFGs for the CTM is higher than the HDTM. It is expected because in the CTM the sub-hourly energy requirement of the power system operation is considered while it is ignored by the HDTM. The main advantage of the CTM is to provide a continuous scheduling for the five cheapest NGFGs to efficiently exploit their ramping capability for tracking the continuous-time changes of the WEGs and load demands, while in the HDTM, the ramping capability is less considered. Therefore, the share of the NGFGs in the generation and fuel consumptions of these generators have been increased. Furthermore, it can be seen from the solution results in Tables III and IV that in the (fuzzy) RA strategy the share of WEGs has been decreased, whereas contrarily the share of the NGFGs in generation has been increased to compensate the wind power deficit, accordingly, the fuel consumptions of these generators have been increased. Likewise, it is observed from this Tables III and IV that the participation of wind farms in the energy procurement has been increased for the (fuzzy) OS strategy, consequently, the share of NGFGs has been reduced. Therefore, the fuel consumptions of these generators have been reduced.

TABLE I: Comparison of results for F-IGDT and IGDT models without EDRP

		Without NGS		With NGS	
		HDTM	CTM	HDTM	CTM
Fuzzy RA	TC	94515.492	80328.521	96350.935	81826.471
	λ	0.228	0.261	0.224	0.256
Fuzzy OS	TC	72766.024	67768.371	73609.582	68494.435
	λ	0.229	0.117	0.248	0.133
RA	TC	96547.204	96547.204	96547.204	96547.204
	λ	0.231	0.634	0.226	0.587
OS	TC	65547.204	65547.204	65547.204	65547.204
	λ	0.338	0.183	0.388	0.25
	Time [min]	1	3	7	11

TABLE II: Comparison of results for F-IGDT and IGDT models with EDRP

		Without NGS		With NGS	
		HDTM	CTM	HDTM	CTM
Fuzzy RA	TC	84117.532	78533.203	85885.626	80006.015
	λ	0.251	0.264	0.242	0.266
Fuzzy OS	TC	66381.839	65657.582	67451.993	66479.595
	λ	0.086	0.07	0.11	0.088
RA	TC	96547.204	96547.204	96547.204	96547.204
	λ	0.682	0.567	0.523	0.635
OS	TC	65547.204	65547.204	65547.204	65547.204
	λ	0.117	0.073	0.179	0.123
	Time [min]	2	5	7	12

TABLE III: Gas consumption of NGFGs without NGS [kcf]

		IGDT				F-IGDT			
		Without EDRP		With EDRP		Without EDRP		With EDRP	
		RA	OS	RA	OS	RA	OS	RA	OS
HDTM	G9	221.2	205.0	221.2	225.5	221.2	217.3	224.7	214.0
	G10	221.2	202.2	221.2	214.0	214.0	211.6	231.2	221.2
	G11	221.2	215.8	223.6	220.7	218.6	210.3	241.2	225.1
	G21	328.7	312.6	333.7	309.1	330.0	310.4	346.9	309.2
	G23	809.7	709.7	827.5	792.5	828.8	717.5	788.7	792.7
	Total	1802.0	1645.3	1827.2	1761.8	1812.7	1667.1	1832.6	1762.2
CTM	G9	227.2	222.6	227.2	223.6	225.7	226.3	223.6	223.6
	G10	227.2	225.3	227.2	224.9	227.2	224.8	227.2	215.5
	G11	229.7	219.6	230.8	226.0	229.1	223.3	237.0	226.5
	G21	331.5	324.6	333.9	329.3	350.6	323.8	345.7	319.9
	G23	816.9	799.2	826.8	804.2	783.5	808.2	774.7	808.4
	Total	1832.6	1791.2	1846.0	1808.1	1816.1	1806.5	1808.3	1793.9

TABLE IV: Gas consumption of NGFGs with NGS [kcf]

		IGDT				F-IGDT			
		Without EDRP		With EDRP		Without EDRP		With EDRP	
		RA	OS	RA	OS	RA	OS	RA	OS
HDTM	G9	116.2	159.2	128.7	164.0	118.6	164.0	111.3	143.0
	G10	109.0	154.1	139.8	132.9	108.1	143.6	124.3	137.3
	G11	115.5	150.6	162.7	141.7	104.8	154.5	123.4	161.4
	G21	302.5	303.5	213.0	277.5	304.0	312.3	305.3	269.5
	G23	569.6	425.1	548.5	436.5	557.2	408.3	508.5	431.4
	Total	1212.7	1192.6	1192.6	1152.6	1192.7	1182.6	1172.7	1142.6
CTM	G9	162.7	140.1	171.3	159.8	149.5	163.5	144.4	144.4
	G10	168.9	152.7	157.3	145.0	143.4	171.5	122.3	134.2
	G11	165.7	140.2	156.9	139.3	134.0	132.7	139.5	162.0
	G21	257.4	307.4	228.0	299.7	326.0	258.6	301.9	300.8
	G23	539.7	464.1	531.0	440.6	551.5	538.1	516.3	443.1
	Total	1294.4	1204.5	1244.5	1184.5	1304.5	1264.5	1224.4	1184.6

3) Impact of EDRP: The effect of discrete-time (DT-EDRP) and continuous-time EDRP (CT-EDRP) in the proposed problem has been studied here. The TEC and λ values associated with the CT-EDRP and DT-EDRP have been reported in Tables I and II. In this test system, the scarcity of ramping capacity is the main obstacle to decrease the TEC and decrease (or increase) λ values. Accordingly, in the condition with no EDRP in the scheduling of the integrated electrical and gas systems, the system would be partially able to cover this scarcity by increasing the share of the NGFGs in generation. Similarly, in the case of availability of EDRP in the scheduling, it can cover this scarcity by ramping capability of the flexible demands. From the data in Tables III and IV, it is apparent that the DT-EDRP and CT-EDRP in (F-) IGDT model can reduce the natural gas consumptions of the five NGFGs, but the CT-EDRP application yields more reduction fuel consumptions than the DT-EDRP. For example, Figs. 7 and 8 compare the natural gas consumptions of the five NGFGs for the DT-EDRP and CT-EDRP in F-IGDT model at each time step. What is interesting about the data in this table is that the hourly natural gas consumption profile is nearly flat when the DT-EDRP and CT-EDRP are incorporated. The differences between the DT-EDRP and CT-EDRP are highlighted in Fig. 8. The most interesting aspect of Fig. 8 is that the profile of the natural gas consumption of the five NGFGs for the CT-EDRP, at peak hours, is more flat than the DT-EDRP. Similarly, further analysis in Fig. 8 showed that the natural gas consumption of the five NGFGs for the CT-EDRP, in peak hours, is more reduced than the DT-EDRP. Taken together, these results suggest that flatter profile of the natural gas consumption at peak hours can reduce the natural gas consumptions of the five NGFGs. While the NGFGs as industrial customers in the natural gas schedule are supplied with lower importance, then their flat profile of natural gas consumption can be managed in a way to avoid having peaks concurrently with residential demands and accordingly it will reduce the probability of inadequate natural gas. It is apparent from Tables I and II that by incorporating the DT-EDRP and CT-EDRP, the amount of required additional WEG (or the λ value) and TEC for (fuzzy) OS strategy is decreased, which means the desired TEC is achieved with the lower levels of actual WEGs. As shown in Tables I and II, the λ and TEC values for the (fuzzy) OS strategy with the CT-EDRP is more reduced than the DT-EDRP. Nevertheless, in the (fuzzy) RA strategy with the DT-EDRP and CT-EDRP, the maximum values of λ and TEC have been increased and reduced, respectively. This shows the fact that by incorporating the EDRP, the acceptable TEC in the (fuzzy) RA strategy is obtained with the higher value of λ. The results of this study indicate that the DT-EDRP and CT-EDRP have positive impacts in both (fuzzy) RA and (fuzzy) OS strategies, since by incorporating EDRP in the (fuzzy) RA strategy the value of λ (the radius of the wind uncertainty) is increased, eventually, while contrarily in the (fuzzy) OS strategy it is decreased. Similarly, by incorporating EDRP, the TEC is decreased, which shows the ability of EDRP for reducing the operation costs in the F-IGDT method. Besides, results in Tables I and II show that the CT-EDRP in (F-) IGDT model, has more effect on the values of λ and TEC. The reason is that in the CTM, the ability to manage the ramping capacity of the NGFGs and flexible demands is more than the DT-EDRP.

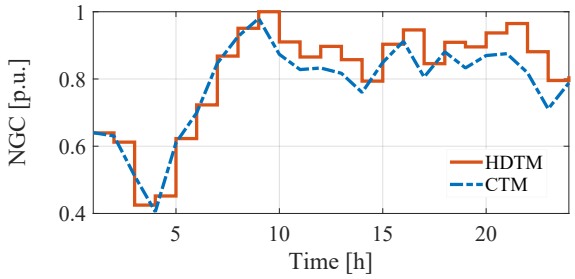

Fig. 7: The natural gas consumption (NGC) of the five NGFGs without the EDRP.

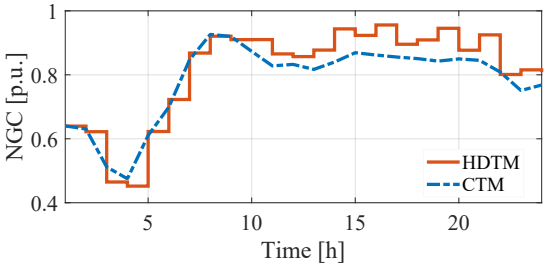

Fig. 8: The natural gas consumption (NGC) of the five NGFGs with the EDRP.

B. Modified IEEE 118-bus system

In other to justify the scalability and reasonable computation complexity of the proposed approach, results of a relatively large-scale system, i.e., modified IEEE-118 bus system, are presented here to represent the computational times required for our proposed approach versus the scale of the test systems. The modified IEEE-118 bus system has 186 transmission lines, 91 load buses, 3 wind farms and 54 thermal generators including 8 natural gas-fired units. Three wind farms with the 250 MW are added to buses 14, 54 and 95. The power output profile of the WF located at three buses follow the same pattern as that of the RTS which is scaled by factor of 2. The peak load of 6000 MW occurs at hour 21. The EDRP at all load buses are considered. The natural gas system consists of 3 suppliers, 12 natural gas loads, and 10 pipelines. L1-L8 are gas loads consumed by NGFGs G1-G8, respectively. L9-L12 are fixed residential gas loads. The detailed data for electricity and natural gas systems have been given in $motor.ece.iit.edu/data/Gastranssmion\_118\_10.xls$. In this section, computational performance of proposed problem (87)-(90) with F-IGDT method, for RA strategy, has been compared with the RM in [14], SM in [13] and IGDT in [17]. In this study, the wind uncertainty model of proposed problem (87)-(90) with (CT) DT-EDRP has been formulated with the RM in [14], SM in [13]. It should be noted that, the RM in [14] has been solved with the primal Benders decomposition algorithm (PBD) in[14].Also, the SM in [13] has been solved with the general Benders decomposition algorithm (GBD) in [25]. For a more detailed formulation of the PBD and GBD, see [13] and [25]. Noted that, the maximum range of wind power uncertainty in RM for each wind farms at time t is fixed to be

0.25%. The wind power uncertainty in the SM pertains to the daily variation of WEG is represented via scenarios and wind uncertainty in SM is fixed to be 0.25%. Approximately, 1500 scenarios are originally generated for SM, being reduced to 20 by the scenario reduction technique proposed in [26]. In this section, the performance of the proposed method and above-mentioned methods have been compared in four aspects: 1) The total cost, 2) The radius of the WEG uncertainty,3) The natural gas consumption of NGFGs,4) Computation time and scalability complexity, The total cost indicates the economic efficiency of the proposed method; the radius of the WEG uncertainty indicates uncertainty management of the proposed method against wind uncertainty; the third aspect indicates how proposed method can reduce the natural gas consumptions for test systems; Final aspect justifies the scalability and reasonable computation complexity of the proposed method. The performances of above-mentioned methods with respect to these three aspects are also compared in Tables V-VI for the CTM and HDTM. It is apparent from Tables V-VI that the proposed F-IGDT method for CTM and HDTM has lower total cost than the RM, SM and IGDT, indicating better economic efficiency of the proposed F-IGDT method. What is interesting about the data in Tables V-VI is that the proposed F-IGDT method has higher λ value and lower total cost than the RM, SM. This result indicate that the proposed F-IGDT method has more capability in wind uncertainty management in lower total cost. Similarly, from the data in Tables V-VI, it is apparent that the natural gas consumption of NGFGs for the proposed F-IGDT method is in lowest level between three methods. This result was expected. However, the reason for this is that the λ value and total cost in the proposed F-IGDT method are optimized simultaneously. For example, for IGDT method just range of wind power uncertainty is optimized, and in the RM just total cost is optimized. Comparing results for the F-IGDT method and the RM in Tables V-VI, it can be seen that the proposed F-IGDT method has higher the λ value and lower total cost than RM. This result was predicted. Nevertheless, it is probable that the reason for this is that in proposed F-IGDT method both λ and total cost values are optimized simultaneously which is ignored in RM. The differences between computation time of proposed F-IGDT method and other methods are highlighted in Tables V-VI. The most surprising aspect of the data in Tables V-VI is that there is a significant difference between the proposed F-IGDT method and SM. The computation time for the proposed F-IGDT method and SM in the 118-bus system is about 22 min and 654 min. However, the computation time increases exponentially in the SM because the SM would introduce additional variables associated with the number of scenarios and increases size of test system. But, the proposed F-IGDT method does not depend on the size of the scenario set. Note that the overall solution time of the proposed F-IGDT method increases with rise the system size. This can be observed from the results presented in Tables V-VI. For instance, comparing the computation time results of the RTS and IEEE 118-bus system for CTM, it becomes evident that the solution time of the IEEE 118-bus system is nearly 2 times larger than the RTS. While the system size increases with a factor of 5 the corresponding solution time does not increase in a linear manner with the system size. What is interesting about the data in Table VI is that for the RM and SM the solution time of the IEEE 118-bus system is nearly 5 times larger than the RTS. Further analysis showed that the corresponding solution time for the SM increases in a linear manner with the system size. Consequently, together these results provide important insights that the SM does not suitable for uncertainty management in large-scale test systems. In CTM for the RTS and IEEE 118-bus system, inputs and outputs are represented with five coefficients in each hour. So, as shown in Tables I-II and V-VI, it is predictable that the computation time and memory consumption is higher for continuous formulation. In other to reduce computation time decomposition or other numerical methods are necessary for implementing this in a fast-paced industrial environment.

TABLE V: Comparison of RA strategy results with the existing methods for HDTM; with EDRP and NGS.

Model	IEEE	TC [M$]	λ	NGC [kfc]	Time [min]
RM	RTS	0.821	0.223	1297.5	21
	118-bus	1.261	0.167	2512.1	101
SM	RTS	0. 959	0.250	1364.4	108
	118-bus	1.358	0.200	3129.8	534
IGDT	RTS	0.965	0.523	1192.6	6
	118-bus	1.350	0.378	2876.5	14
F-IGDT	RTS	0.812	0.254	1142.6	7
	118-bus	1.256	0.187	2678.5	18

TABLE VI: Comparison of RA strategy results with the existing methods for CTM; with EDRP and NGS.

Model	IEEE	TC [M$]	λ	NGC [kfc]	Time [min]
RM	RTS	0.808	0.248	1229.2	34
	118-bus	1.244	0.187	2467.5	154
SM	RTS	0. 955	0.250	1328.2	234
	118-bus	1.356	0.200	2967.3	654
IGDT	RTS	0. 965	0.635	1244.5	9
	118-bus	1.350	0.442	2456.7	21
F-IGDT	RTS	0.800	0.266	1224.4	12
	118-bus	1.234	0.212	2456.7	22

VII. Conclusions

This paper has developed a new F-IGDT framework for co-operation of electric power system with natural gas system in the discrete-time and continuous-time modeling methods, while considering the uncertainty of WEGs. Both interdependent systems of natural gas and electric power are linked with the NGFGs. In this study, a full frame NGS is considered to address the dispatchability of the NGFGs, which can play a vital role in providing a fast ramping in electric power systems to follow the fast variations of the WEGs. However, the natural gas supply limitation is the main obstacle to provide the fast ramping capability. Nevertheless, such limitations can be significantly moderated by means of EDRPs. In this study, the EDRP as an appropriate economic solution has been used as a complementary option for providing the ramping facility beside the NGFGs in the case of an unavailability of natural gas. Also, this study aims to determine whether the continuous-time framework can positively affect the co-

operation of electric power and natural gas systems. The simulations on the IEEE-RTS and IEEE 118-bus system imply that the proposed continuous-time framework reveals a continuous-time scheduling of NGFGs and EDRP, which more efficiently utilizes their ramping capability to track the continuous-time changes of the WEGs and load demands than the discrete-time framework. Accordingly, the obtained results confirm that the proposed continuous-time framework, in comparison to the discrete-time framework, provides additional decrease in the TEC and increase in the λ for both (fuzzy) RA and OS strategies. Also, in this study, the performance of the proposed method and the RM, SM and IGDT method have been compared on the IEEE-RTS and IEEE 118-bus system in four aspects: i) The economic efficiency, ii) The uncertainty management, iii) The natural gas consumption, iv) computation time and scalability complexity. Consequently, results provide important insights that the proposed F-IGDT method has more economic efficiency, more capability in wind uncertainty management in lower total cost, more saving natural gas energy, and lower computation complexity with scalability than other methods.

APPENDIX A:LINEARIZATION WEYMOUTH EQUATION

The nonlinear Weymouth equation or pipeline flow rate constraints without gas compressor would have a significant impact on the computation complexity of the proposed problem. In this paper, we convert nonlinear Weymouth equation into a set of linear constraints by using piecewise linear approximation, which is briefly discussed below. The lower and upper limits of gas pressure in each nodal are modeled as [10]:

$$\underline{\pi}_i \leq \pi_{it} \leq \overline{\pi}_i \tag{91}$$

The nonlinear Weymouth equation [10]:

$$f_{pt}^2 = \Theta_p \left(\pi_{it}^2 - \pi_{jt}^2\right) \tag{92}$$

The square of node pressure is expressed as:

$$\rho_{it} = \pi_{it}^2 \tag{93}$$

To improve the linearity of the proposed model, π_{it}^2 in Equation (92) is replaced with square of node pressure ρ_{it} and Equation (92) is reformulated as:

$$f_{pt}^2 = \Theta_p \left(\rho_{it} - \rho_{jt}\right) \tag{94}$$

Then, the piecewise linear approximation of f_{pt}^2 in Equation (94) written as follow:

$$\sum_{\ell} \left(\varphi_{\ell,p} \cdot f_{\ell,pt} + \gamma_{p,\ell} \cdot \nu_{\ell,pt}\right) = \Theta_p \left(\rho_{it} - \rho_{jt}\right) \tag{95}$$

where $\varphi_{\ell,p}$,$\gamma_{p,\ell}$ and Θ_p are constants in the piecewise linear approximation for the ℓth linear block; ρ_{it} and ρ_{jt} are node pressures; and $\nu_{\ell,pt}$ is binary indicator variable. The following linear constraints are introduced based on the preceding notations:

$$\nu_{\ell,pt} \cdot \underline{f}_{\ell,p} \leq f_{\ell,pt} \leq \nu_{\ell,pt} \cdot \overline{f}_{\ell,p} \tag{96}$$

$$f_{pt} = \sum_{\ell} f_{\ell,pt} \tag{97}$$

$$\sum_{\ell} \nu_{\ell,pt} \leq 1 \tag{98}$$

Equations (96) – (98) are defined before in detail. The more detailed about this linearization is given in [10]. Noted that, the linearization of pipeline flow rate equation without gas compressor is similar to nonlinear Weymouth equation.

REFERENCES

[1] U.S. National Renewable Energy Laboratory, 20% Wind Energy by 2030: IncreasingWind Energy's Contribution to U.S. Electricity Supply[Online]. Available: http:// www.nrel.gov/docs/fy08osti/41869.pdf.

[2] M. Shahidehpour, Y. Fu, and T. Wiedman, "Impact of natural gas infrastructure on electric power systems," Proceedings of the IEEE, vol. 93, no. 5, pp. 1042-1056, 2005.

[3] G. Li, R. Zhang, T. Jiang, H. Chen, L. Bai, and X. Li, "Security-constrained bi-level economic dispatch model for integrated natural gas and electricity systems considering wind power and power-to-gas process," Applied energy, vol. 194, pp. 696-704, 2017.

[4] T. D. Diagoupis, P. E. Andrianesis, and E. N. Dialynas, "A planning approach for reducing the impact of natural gas network on electricity markets," Applied Energy, vol. 175, pp. 189-198, 2016.

[5] T. Li, M. Eremia, and M. Shahidehpour, "Interdependency of natural gas network and power system security," IEEE Transactions on Power Systems, vol. 23, no. 4, pp. 1817-1824, 2008.

[6] C. Liu, M. Shahidehpour, and J. Wang, "Application of augmented Lagrangian relaxation to coordinated scheduling of interdependent hydrothermal power and natural gas systems," IET Generation, Transmission & Distribution, vol. 4, no. 12, pp. 1314-1325, 2010.

[7] C. M. Correa-Posada and P. Sánchez-Martín, "Integrated power and natural gas model for energy adequacy in short-term operation," IEEE Transactions on Power Systems, vol. 30, no. 6, pp. 3347-3355, 2015.

[8] C. Liu, M. Shahidehpour, Y. Fu, and Z. Li, "Security-constrained unit commitment with natural gas transmission constraints," IEEE Trans. Power Syst, vol. 24, no. 3, pp. 1523-1536, 2009.

[9] L. Wu and M. Shahidehpour, "Optimal coordination of stochastic hydro and natural gas supplies in midterm operation of power systems," IET generation, transmission & distribution, vol. 5, no. 5, pp. 577-587, 2011.

[10] A. Alabdulwahab, A. Abusorrah, X. Zhang, and M. Shahidehpour, "Stochastic security-constrained scheduling of coordinated electricity and natural gas infrastructures," IEEE Systems Journal, vol. 11, no. 3, pp. 1674-1683, 2017.

[11] A. Antenucci and G. Sansavini, "Gas-Constrained Secure Reserve Allocation With Large Renewable Penetration," IEEE Transactions on Sustainable Energy, vol. 9, no. 2, pp. 685-694, 2018.

[12] M. Parvania and A. Scaglione, "Generation ramping valuation in day-ahead electricity markets," in System Sciences (HICSS), 2016 49th Hawaii International Conference on, 2016, pp. 2335-2344: IEEE.

[13] J. Aghaei, A. Nikoobakht, P. Siano, M. Nayeripour, A. Heidari, and M. Mardaneh, "Exploring the reliability effects on the short term AC security-constrained unit commitment: A stochastic evaluation," Energy, vol. 114, pp. 1016-1032, 2016.

[14] D. Bertsimas, E. Litvinov, X. A. Sun, J. Zhao, and T. Zheng, "Adaptive robust optimization for the security constrained unit commitment problem," IEEE Transactions on Power Systems, vol. 28, no. 1, pp. 52-63, 2013.

[15] C. He, L. Wu, T. Liu, and Z. Bie, "Robust co-optimization planning of interdependent electricity and natural gas systems with a joint N-1 and probabilistic reliability criterion," IEEE Transactions on Power Systems, vol. 33, no. 2, pp. 2140-2154, 2017.

[16] C. He, L. Wu, T. Liu, and M. Shahidehpour, "Robust co-optimization scheduling of electricity and natural gas systems via ADMM," IEEE Transactions on Sustainable Energy, vol. 8, no. 2, pp. 658-670, 2017.

[17] A. Nikoobakht and J. Aghaei, "IGDT-based robust optimal utilisation of wind power generation using coordinated flexibility resources," IET Renewable Power Generation, vol. 11, no. 2, pp. 264-277, 2016.

[18] M. A. Mirzaei, A. S. Yazdankhah, B. Mohammadi-Ivatloo, M. Marzband, M. Shafie-khah, and J. P. Catalão, "Integration of emerging resources in IGDT-based robust scheduling of combined power and natural gas systems considering flexible ramping products," Energy, p. 116195, 2019.

[19] F. Sohrabi, F. Jabari, B. Mohammadi-Ivatloo, and A. Soroudi, "Co-ordination of interdependent natural gas and electricity systems based on information gap decision theory," IET Generation, Transmission & Distribution, vol. 13, no. 15, pp. 3362-3369, 2019.

[20] M. Sakawa, Fuzzy sets and interactive multiobjective optimization. Springer Science & Business Media, 2013.

[21] M. Parvania and A. Scaglione, "Unit commitment with continuous-time generation and ramping trajectory models," IEEE Transactions on Power Systems, vol. 31, no. 4, pp. 3169-3178, 2015.
[22] R. Khatami, M. Parvania, and K. Oikonomou, "Continuous-time optimal charging control of plug-in electric vehicles," in 2018 IEEE Power & Energy Society Innovative Smart Grid Technologies Conference (ISGT), 2018, pp. 1-5: IEEE.
[23] R. Khatami, M. Parvania, and P. Khargonekar, "Continuous-time Look-Ahead Scheduling of Energy Storage in Regulation Markets," in Proceedings of the 52nd Hawaii International Conference on System Sciences, 2019.
[24] M. Parvania and R. Khatami, "Continuous-time marginal pricing of electricity," IEEE Transactions on Power Systems, vol. 32, no. 3, pp. 1960-1969, 2016.
[25] P. Dierckx, Curve and surface fitting with splines. Oxford University Press, 1995.
[26] P. M. Prenter, Splines and variational methods. Courier Corporation, 2008.
[27] R. T. Force, "The IEEE reliability test system-1996," IEEE Trans. Power Syst, vol. 14, no. 3, pp. 1010-1020, 1999.
[28] motor.ece.iit.edu/data/Gas transsmion_118_10.xls.
[29] R. Rahmaniani, T. G. Crainic, M. Gendreau, and W. Rei, "The Benders decomposition algorithm: A literature review," European Journal of Operational Research, vol. 259, no. 3, pp. 801-817, 2017.
[30] J. M. Morales, S. Pineda, A. J. Conejo, and M. Carrion, "Scenario reduction for futures market trading in electricity markets," IEEE Transactions on Power Systems, vol. 24, no. 2, pp. 878-888, 2009.

Ahmad Nikoobakht was born in Iran in 1988. He received the B.Sc. degree in electrical engineering from Hormozgan University, Iran, in 2011, and the M.Sc. and Ph.D. degrees from Shiraz University of Technology, Shiraz, Iran, in 2013 and 2017, respectively. He is currently an Assistance Professor in the Electrical Engineering Department of Higher Education Center of Eghlid, Eghlid, Iran. His research interests include renewable energy systems, smart grids, electricity markets, electric vehicle, demand response, energy storage systems, FACTS devices and optimal planning and operation of power systems, as well as statistics and optimization theory and its applications.

Jamshid Aghaei (M'12–SM'15) received the B.Sc. degree in electrical engineering from the Power and Water Institute of Technology, Tehran, Iran, in 2003, and the M.Sc. and Ph.D. degrees from the Iran University of Science and Technology, Tehran, in 2005 and 2009, respectively. He is currently a Full Professor with the Shiraz University of Technology, Shiraz, Iran. His research interests include renewable energy systems, smart grids, electricity markets, and power system operation, optimization, and planning.

He is a member of the Iranian Association of Electrical and Electronics Engineers, an Associate Editor for the IET Renewable Power Generation, a Subject Editor of IET Generation Transmission and Distribution, an Editor of IEEE Open Access Journal of Power and Energy, and a Guest Editor of the IEEE TRANSACTIONS ON INDUSTRIAL INFORMATICS. He was considered one of the outstanding reviewers of the IEEE TRANSACTIONS ON SUSTAINABLE ENERGY, in 2017.

Miadreza Shafie-khah (M'13-SM'17)received the M.Sc. and Ph.D. degrees in electrical engineering from Tarbiat Modares University, Tehran, Iran, in 2008 and 2012, respectively. He received his first postdoc from the University of Beira Interior (UBI), Covilha, Portugal in 2015. He received his second postdoc from the University of Salerno, Salerno, Italy in 2016. Currently, he is a Tenure-Track Professor at the University of Vaasa, Vaasa, Finland. He is currently an Associate Editor for IET-RPG and an editor of the IEEE OAJPE. He was considered one of the Outstanding Reviewers of the IEEE TRANSACTIONS ON SUSTAINABLE ENERGY, in 2014 and 2017, one of the Best Reviewers of the IEEE TRANSACTIONS ON SMART GRID, in 2016 and 2017, and one of the Outstanding Reviewers of the IEEE TRANSACTIONS ON POWER SYSTEMS, in 2017 and 2018. His research interests include power market simulation, market power monitoring, power system optimization, demand response, electric vehicles, price forecasting and smart grids.

Jolão P. S. Catalão (M'04-SM'12) received the M.Sc. degree from the Instituto Superior Técnico (IST), Lisbon, Portugal, in 2003, and the Ph.D. degree and Habilitation for Full Professor ("Agregação") from the University of Beira Interior (UBI), Covilha, Portugal, in 2007 and 2013, respectively. Currently, he is a Professor at the Faculty of Engineering of the University of Porto (FEUP), Porto, Portugal, and Research Coordinator at INESC TEC. He was also appointed as Visiting Professor by North China Electric Power University, Beijing, China. He was the Primary Coordinator of the EU-funded FP7 project SiNGULAR ("Smart and Sustainable Insular Electricity Grids Under Large-Scale Renewable Integration"), a 5.2-million-euro project involving 11 industry partners. He has authored or coauthored more than 750 publications, including 325 journal papers (more than 90 IEEE Transactions/Journal papers), 366 conference proceedings papers, 5 books, 40 book chapters, and 14 technical reports, with an h-index of 56, an i10-index of 246, and over 11,775 citations (according to Google Scholar), having supervised more than 70 post-docs, Ph.D. and M.Sc. students. He was the General Chair of SEST 2019 (2nd International Conference on Smart Energy Systems and Technologies), technically sponsored by IEEE PES and IEEE IES. He is the General Co-Chair of SEST 2020 (3rd International Conference on Smart Energy Systems and Technologies), technically sponsored by IEEE PES, IEEE IES and IEEE IAS. He is the Editor of the books entitled "Electric Power Systems: Advanced Forecasting Techniques and Optimal Generation Scheduling" and "Smart and Sustainable Power Systems: Operations, Planning and Economics of Insular Electricity Grids" (Boca Raton, FL, USA: CRC Press, 2012 and 2015, respectively). His research interests include power system operations and planning, hydro and thermal scheduling, wind and price forecasting, distributed renewable generation, demand response and smart grids. Prof. Catalão is the Promotion and Outreach Editor of the new IEEE OPEN ACCESS JOURNAL OF POWER AND ENERGY, an Editor of the IEEE TRANSACTIONS ON SMART GRID, an Editor of the IEEE TRANSACTIONS ON POWER SYSTEMS, and an Associate Editor of the IEEE TRANSACTIONS ON INDUSTRIAL INFORMATICS. From 2011 till 2018 he was an Editor of the IEEE TRANSACTIONS ON SUSTAINABLE ENERGY and an Associate Editor of the IET Renewable Power Generation. He was also a Subject Editor of the IET Renewable Power Generation from 2018 till 2019. He was the Guest Editor-in-Chief for the Special Section on "Real-Time Demand Response" of the IEEE TRANSACTIONS ON SMART GRID, published in December 2012, the Guest Editor-in-Chief for the Special Section on "Reserve and Flexibility for Handling Variability and Uncertainty of Renewable Generation" of the IEEE TRANSACTIONS ON SUSTAINABLE ENERGY, published in April 2016, the Corresponding Guest Editor for the Special Section on "Industrial and Commercial Demand Response" of the IEEE TRANSACTIONS ON INDUSTRIAL INFORMATICS, published in November 2018, and the Lead Guest Editor for the Special Issue on "Demand Side Management and Market Design for Renewable Energy Support and Integration" of the IET Renewable Power Generation, published in April 2019. He was the recipient of the 2011 Scientific Merit Award UBI-FE/Santander Universities, the 2012 Scientific Award UTL/Santander Totta, the 2016-2017-2018 FEUP Diplomas of Scientific Recognition, the 2017 Best INESC-ID Researcher Award, and the 2018 Scientific Award ULisboa/Santander Universities, in addition to an Honorable Mention in the 2017 Scientific Award ULisboa/Santander Universities. Moreover, he has won 4 Best Paper Awards at IEEE Conferences.